LYMPHATIC RESEARCH AND BIOLOGY
Volume 13, Number 2, 2015

DOI: 10.1089/lrb.2014.0009

Lymphatic Stomata in the Adult Human Pulmonary Ligament

Hisashi Oshiro, MD, PhD,[1,5] Masahiro Miura, PhD,[2] Hiroaki Iobe, LT,[1] Tomoo Kudo, DVM, PhD,[4,*] Yoshihito Shimazu, PhD,[4,§] Takaaki Aoba, DDS, PhD,[4] Koji Okudela, MD, PhD,[5] Kiyotaka Nagahama, MD, PhD,[5] Kentaro Sakamaki, PhD,[6] Maki Yoshida, DDS, PhD,[1] Toshitaka Nagao, MD, PhD,[1] Takeo Nakaya, MD, PhD,[3] Atsushi Kurata, MD, PhD,[3] and Osamu Ohtani, MD, PhD[7]

Abstract

Background: Lymphatic stomata are small lymphatic openings in the serosal membrane that communicate with the serosal cavity. Although these stomata have primarily been studied in experimental mammals, little is known concerning the presence and properties of lymphatic stomata in the adult human pleura. Thus, adult human pleurae were examined for the presence or absence of lymphatic stomata.

Methods and Results: A total of 26 pulmonary ligaments (13 left and 13 right) were obtained from 15 adult human autopsy cases and examined using electron and light microscopy. The microscopic studies revealed the presence of apertures fringed with D2-40-positive, CD31-positive, and cytokeratin-negative endothelial cells directly communicating with submesothelial lymphatics in all of the pulmonary ligaments. The apertures' sizes and densities varied from case to case according to the serial tissue section. The medians of these aperture sizes ranged from 2.25 to 8.75 μm in the left pulmonary ligaments and from 2.50 to 12.50 μm in the right pulmonary ligaments. The densities of the apertures ranged from 2 to 9 per mm^2 in the left pulmonary ligaments and from 2 to 18 per mm^2 in the right pulmonary ligaments. However, no significant differences were found regarding the aperture size ($p=0.359$) and density ($p=0.438$) between the left and the right pulmonary ligaments.

Conclusions: Our study revealed that apertures exhibit structural adequacy as lymphatic stomata on the surface of the pulmonary ligament, thereby providing evidence that lymphatic stomata are present in the adult human pleura.

Introduction

The factors that influence fluid turnover in the serosal cavity of mammals include the following: 1) Starling's hypothesis (the transcapillary hydrostatic pressure gradient is opposed by the colloid osmotic pressure gradient multiplied by the capillary ultrafiltration coefficient); 2) Fick's law of diffusion; 3) the serosal pressure associated with organ movement and posture, whether passive or active; 4) active transport by the mesothelial cells; and 5) a lymphatic drainage system via the lymphatic stomata.[1,2] Of these factors, the lymphatic drainage system via the lymphatic stomata is considered to play an important role, contributing up to approximately 75%–80% of the fluid absorption rate in the serosal cavity.[1–6]

Lymphatic stomata are small openings that enable direct communication between the lymphatic lumen and the serosal cavity.[7] Since apertures in the diaphragmatic peritoneum were first described,[8] numerous investigators have confirmed the existence of lymphatic stomata not only in the peritoneum but also in the pleura of various types of mammals, such as rabbits,[9] rats,[9–11] sheep,[12,13] monkeys,[14,15] golden hamsters,[16] and mice.[17] A large proportion of the liquid in the pleural cavity is presumed to exit by bulk flow not by diffusion or active transport.[5] Because erythrocytes within the pleural cavity are absorbed intact and in almost the same proportion as the liquid and protein,[18] Broaddus and Light predicted the existence of a major exit route via holes large enough to accommodate sheep erythrocytes (diameter, 6–8 μm), making the pleural stomata the only possible exit

Departments of [1]Anatomic Pathology and [3]Molecular Pathology, Tokyo Medical University, Tokyo, Japan.
[2]Department of Human Anatomy, Oita University, Oita, Japan.
[4]Department of Pathology, Nippon Dental University, Tokyo, Japan.
Departments of [5]Pathology and [6]Biostatistics and Epidemiology, Yokohama City University Graduate School of Medicine, Yokohama, Japan.
[7]Department of Anatomy, University of Toyama Graduate School of Medicine and Pharmaceutical Sciences, Toyama, Japan.
*Tomoo Kudo is now with the Department of Pathology, Hyogo College of Medicine, Hyogo, Japan.
§Yoshihito Simazu is now with the Department of Food and Life Sciences, Azabu University, Kanagawa, Japan.

Table 1. Clinicopathological Features of 15 Autopsy Cases

					Left-sided pleural cavity				*Right-sided pleural cavity*			
Case	*Sex*	*Age (year)*	*Main disease*	*Time after death (hour)*	*Length of the pulmonary ligament (mm)*	*Number of lymph node #9 (maximum diameter)*	*Volume of pleural effusion (ml)*	*Malignant pleural effusion*	*Length of the pulmonary ligament (mm)*	*Number of lymph node #9 (maximum diameter)*	*Volume of pleural effusion (ml)*	*Malignant pleural effusion*
1	man	73	Bile duct cancer	3.10	80	3 (12 mm)	800	negative	65	1 (12 mm)	750	negative
2	man	50	Sigmoid colon cancer	2.16	50	1 (3 mm)	15	negative	50	1 (2 mm)	25	negative
3	man	67	Pancreatic cancer	1.83	60	5 (8 mm)	0	negative	63	3 (8 mm)	0	negative
4	woman	53	Rectal cancer	2.60	72	2 (5 mm)	230	negative	70	2 (3 mm)	870	negative
5	man	68	Pancreatic cancer	3.00	75	0	2	negative	55	1 (2 mm)	10	negative
6	man	85	Liver cancer	2.50	57	0	30	negative	51	0	10	negative
7	man	66	Kidney cancer	3.50	55	1 (2 mm)	940	negative	55	2 (1 mm)	460	negative
8	man	48	Colon cancer, Sepsis	4.50	58	1 (3 mm)	200	negative	53	2 (5 mm)	230	negative
9	man	43	AIDS	2.50	55	0	350	negative	60	0	850	negative
10	man	83	Ischemic small intestinitis	2.10	76	0	420	negative	66	0	370	negative
11	man	72	Pneumonia, Hepatitis B	2.38	65	1 (5 mm)	500	negative	52	0	500	negative
12	man	57	Acute myeloid leukemia (M5a)	4.48	n/e	n/e	n/e	n/e	51	5 (10 mm)	620	positive
13	woman	73	Lung cancer	2.50	60	0	50	negative	n/e	n/e	n/e	n/e
14	man	70	Lung cancer	4.00	n/e	n/e	n/e	n/e	45	1 (5 mm)	650	negative
15	man	89	Pneumonia	2.78	64	0	3	negative	n/e	n/e	n/e	n/e

n/e = not evaluated because of pleural adhesion.

(diameter, 10–12 μm) into the pleural lymphatics.[5] However, these stomata have not been established in the adult human pleura.[19] Gaudio et al. studied visceral, mediastinal, diaphragmatic, and costal pleural samples obtained from 30 human adults, but they were unable to assess lymphatic stomata.[20] Peng et al. observed several gaps between mesothelial cells in two of eleven adult human parietal pleural samples; however, it is uncertain whether these gaps directly communicated with the submesothelial lymphatics in their study.[21] Liu et al. reported that the adult human pulmonary ligaments were characterized by the presence of stomata;[22] however, their study did not demonstrate lymphatic stomata properties. The lack of morphological evidence of lymphatic stomata prompted us to examine the adult human pleura.

The pulmonary ligament is a double-layered structure of pleura that connects the visceral pleura on the lower medial aspect of the lung to the parietal pleura on the mediastinum. The ligament extends downward in a sheet-like manner from the level of the lower pulmonary vein toward the diaphragmatic pleura, where it either is fixed or terminates in a free falciform border.[23] The aim of this study was to ascertain the presence of lymphatic stomata in the adult human pulmonary ligament.

Materials and Methods

Adult human autopsy cases encountered at Yokohama City University Hospital and Tokyo Medical University Hospital between 2004 and 2012 were examined in the present study. The criteria for inclusion in the study were as follows: 1) autopsy was conducted within 5 hours after death, and 2) pulmonary ligaments were grossly intact and free from adhesion. Twenty-six pulmonary ligaments (13 left and 13 right) were obtained from 15 Japanese cadavers (13 men and 2 women; mean age, 66.5 years) and were eligible for inclusion in the study. The clinicopathological features are summarized in Table 1. After gross examination, the pulmonary ligaments were gently excised without touching the surface; cut into small portions along a horizontal (short axis) direction; and fixed in 10%–20% neutral-buffered formalin

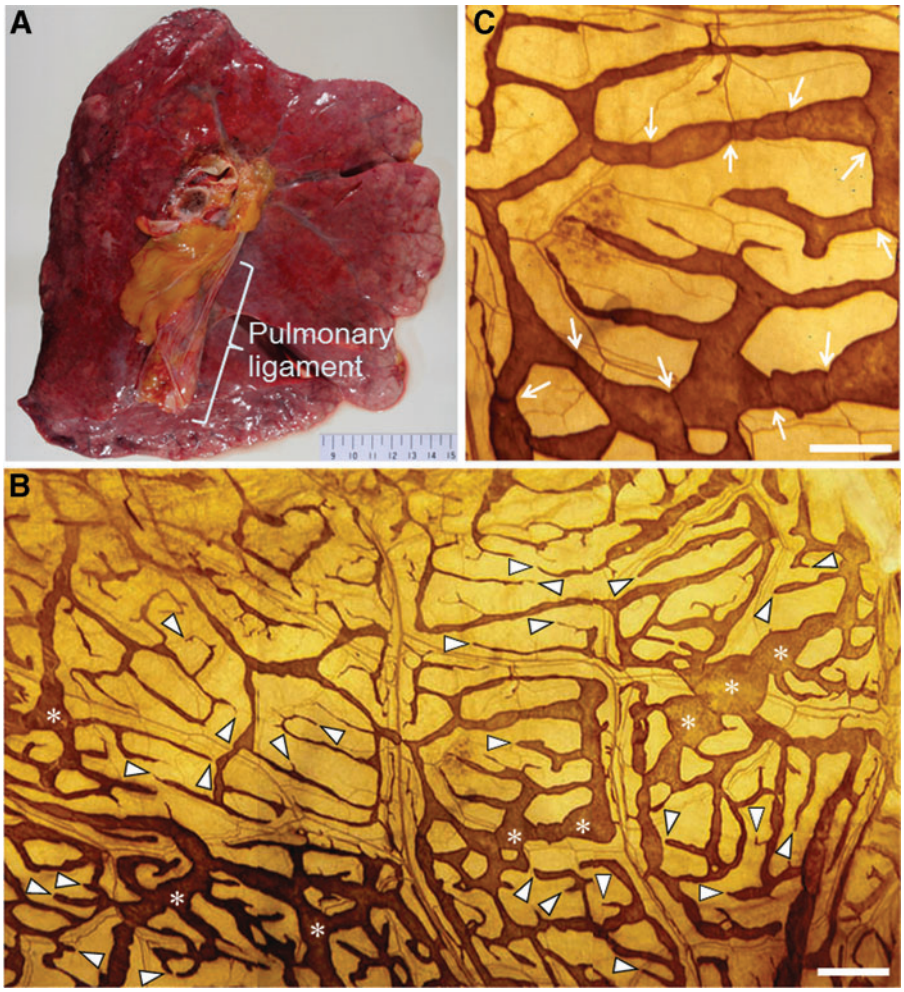

FIG. 1. **(A)** A macroscopic image of the mediastinal side of the left lung demonstrating the pulmonary ligament. **(B)** A panel of three photomicrographs of 5′-nucleotidase enzyme histochemistry performed on the surface side of the extended material of the human pulmonary ligament. Brown-colored, lattice-like lymphatic networks are visible along with numerous blind-ended initial lymphatics (*arrowheads*) and irregularly dilated lymphatics (*asterisks*). The scale bar indicates 500 μm. **(C)** A high-power view photomicrograph of (B). Ill-defined valve-like structures can be observed (*arrows*). The scale bar indicates 250 μm. A color version of this figure is available in the online article at www.liebertpub.com/lrb

for histological and immunohistochemical studies, 4% paraformaldehyde for enzyme histochemistry, and 2.5% glutaraldehyde in 0.1 mol/L cacodylate buffer for ultrastructural studies. The upper and middle regions of the pulmonary ligament were mainly used for enzyme histochemistry, whereas the lower region was mainly used for electron microscopic and immunohistochemical studies.

After fixation for 3 days at 4° Celsius, enzyme histochemistry was performed using 5′-nucleotidase to investigate the submesothelial lymphatics of the pulmonary ligament according to the method described previously.[24]

Ultrastructural studies were performed as follows. After glutaraldehyde fixation, the samples were postfixed in cacodylate-buffered 2% osmium tetroxide for 2 h, dehydrated in ethanol, and subsequently dried using the *t*-butyl alcohol freeze-drying method.[11] The specimens were sputter-coated with gold and observed under a scanning electron microscope (S-4800; Hitachi; Tokyo, Japan).[11] Transmission electron microscopy was also conducted under a microscope (H-7500; Hitachi).[25]

A light microscopic study was performed using serial 2-μm tissue sections obtained from formalin-fixed, paraffin-embedded tissue blocks; 50 serial sections per sample were used for hematoxylin and eosin staining and immunohistochemistry in series. Immunohistochemistry was performed using an autostainer (Histostainer, Nichirei, Tokyo, Japan), antibodies against cytokeratin CAM5.2 (CAM5.2, mouse IgG2a, Becton Dickinson, San Jose, CA, USA) as a marker for mesothelial cells, D2-40 (equal to podoplanin) (D2-40, mouse IgG1, Signet Laboratories, Dedham, MA, USA) as a marker for lymphatic endothelial cells and mesothelial cells and CD31 (JC/70A, Dako, Glostrup, Denmark) as a marker for lymphatic and blood vascular endothelial cells, and a detection kit (Histofine Simple Stain MAX PO, MULTI, Nichirei) according to the manufacturers' instructions. The alveolar epithelium and the lymphatic and blood vascular endothelia of the lung were used as positive controls for the immunohistochemistry. For negative controls, the primary antibodies were omitted during the staining procedure.

Indirect immunofluorescence was performed using a double-staining method for CAM5.2 with Alexa Fluor 488-conjugated goat anti-mouse IgG2a antibody (Invitrogen, Carlsbad, CA, USA), and D2-40 with Alexa Fluor 555-conjugated goat anti-mouse IgG1 antibody (Invitrogen) as well as 4′,6-diamidino-2-phenylindole (DAPI) (Roche Diagnostics, Mannheim, Germany).[26] To observe the immunofluorescent images, a fluorescence microscope (BX51, Olympus, Tokyo, Japan) was employed.

Three-dimensional histological image reconstruction was performed using serial tissue sections stained with CAM5.2 and D2-40 antibodies, a virtual slide scanner system (Nanozoomer 2.0RS, Hamamatsu Photonics, Hamamatsu, Japan), and TRI/3D-SRF2 software (Ratoc System Engineering, Tokyo, Japan).[27]

From the serial tissue sections, the sizes and frequencies of the apertures fringed with endothelial cells and directly connected to the pleural cavity with submesothelial lymphatics were measured over approximately 1-mm^2 regions of serosa. The sizes and frequencies of apertures between the right and left pulmonary ligaments were compared using a paired Wilcoxon rank sum test with SPSS 18.0 (SPSS, Chicago, IL, USA).

Results

Enzyme histochemistry with 5′-nucleotidase revealed a rich submesothelial lymphatic network in the pulmonary ligament (Fig. 1). Lattice-like lymphatic networks were visible with numerous blind-ended initial lymphatics and irregularly dilated lymphatics. The fractions (area densities) of these superficial lymphatics were approximately 25%–35%. The dimensions of these superficial lymphatics varied greatly (1–420 μm). Ill-defined valve-like structures were observed in these superficial lymphatics. The dimensions of the initial lymphatics ranged from approximately 1 to 4 μm.

Scanning electron microscopy revealed primarily three types of serosal membranes in the pulmonary ligament: 1) flattened with scarce microvilli; 2) intermediate; and 3) cuboidal and microvilli-rich mesothelial cells (Fig. 2). The membranes composed of cuboidal and microvilli-rich mesothelial cells tended to accompany several apertures between them. However, the shapes and sizes of these apertures were diverse. Some apertures were circular, whereas others

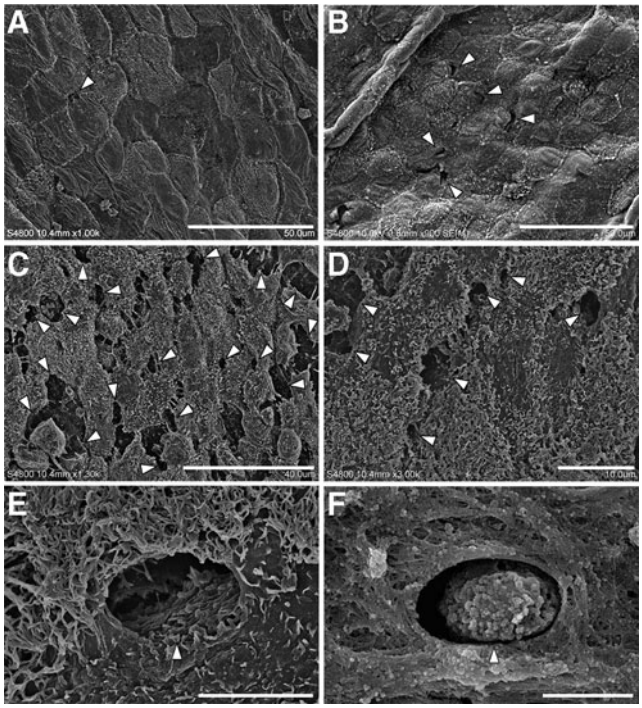

FIG. 2. Scanning electron micrographs of the surface side of the pulmonary ligament. **(A)** Serosal membrane composed of flattened mesothelial cells. Several small apertures (*arrowhead*) can be observed between the mesothelial cells. The scale bar indicates 50 μm. **(B)** Serosal membrane composed of intermediate mesothelial cells. Several small stomata (*arrowheads*) can be observed. The scale bar indicates 50 μm. **(C)** Serosal membrane composed of cuboidal mesothelial cells. A large number of stomata (*arrowheads*) or gaps can be observed. The scale bar indicates 40 μm. **(D)** Circular or irregularly shaped stomata (*arrowheads*) with deep furrows. The scale bar indicates 10 μm. **(E)** A circular stoma (*arrowhead*) surrounded by cuboidal mesothelial cells characterized by prominent microvilli. A submesothelial tissue structure can be noted at the bottom of the stoma. The scale bar indicates 5 μm. **(F)** An arrowhead indicates a cell passing through the stoma. The scale bar indicates 4.3 μm.

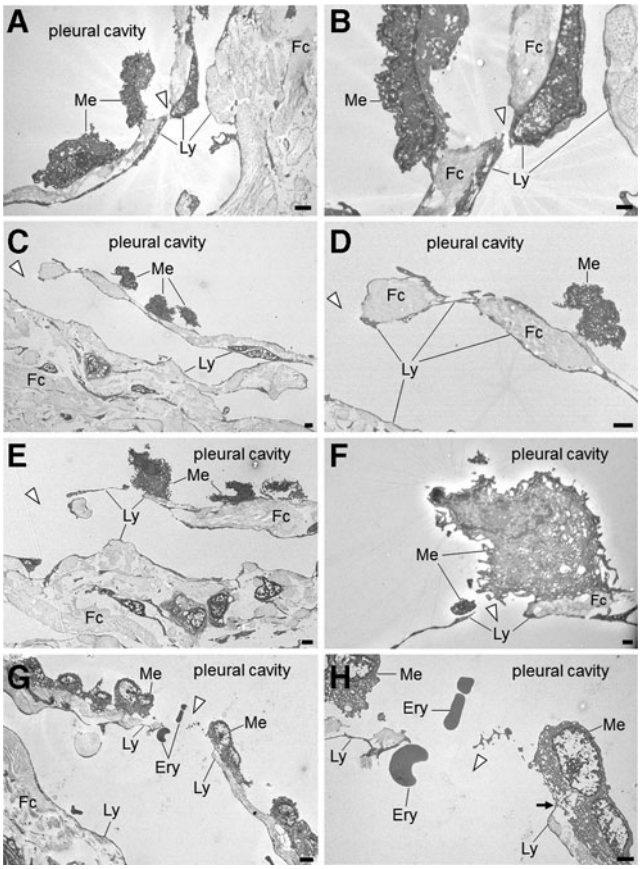

FIG. 3. Transmission electron micrographs of the pulmonary ligament. Panels on the right side are enlargements of details presented in the panels on the left. **(A)** Cuboidal mesothelial cells can be observed on the surface of the serosal membrane. The submesothelial layer consists of fibrous connective tissue, which is discontinuous and interrupted by a stoma (*arrowhead*). The scale bar indicates 2 μm. **(B)** A stoma (*arrowhead*) surrounded by cytoplasm of lymphatic endothelial cells. The scale bar indicates 0.5 μm. **(C)** A stoma directly continuing into a lymphatic capillary (*arrowhead*). The scale bar indicates 2 μm. **(D)** A stoma (*arrowhead*) and lymphatic endothelial cells surrounding fibrous connective tissue and directly exposed to the pleural cavity. The scale bar indicates 2 μm. **(E)** A stoma (*arrowhead*) directly continuing into a lymphatic capillary. The scale bar indicates 2 μm. **(F)** A stoma composed of thin cytoplasm of a lymphatic endothelial cell adjacent to a mesothelial cell. The scale bar indicates 0.5 μm. **(G)** A stoma (*arrowhead*) directly continuing into a lymphatic capillary and erythrocytes passing through a stoma. The scale bar indicates 5 μm. **(H)** A stoma fringed with lymphatic endothelial cells (*arrowhead*). On the right side of the stoma, a lymphatic endothelial cell is in contact with a mesothelial cell (*arrow*). The scale bar indicates 2 μm. Ery, erythrocyte; Fc, fibrous connective tissue; Ly, lymphatic endothelial cell; Me, mesothelial cell.

were irregular; some were small or narrow, such as clefts, whereas others were large enough for a cell to pass through. Gullies on the pleural surface were often too deep and dark to determine whether these apertures continued to the submesothelial lymphatic lumen. Measuring the precise size of the apertures was difficult due to their irregular shapes.

Transmission electron microscopy revealed the presence of apertures in the serosal membranes that directly communicate with submesothelial lymphatic capillaries (Fig. 3). The orifices of these apertures were fringed with cytoplasmic elongation of submesothelial lymphatic endothelial cells. The sizes of these apertures were diverse; several apertures were small with overlapping endothelial cells, whereas others were large enough for a cell to pass through and did not exhibit overlapping endothelial cells.

Our histological study revealed that the surface of the pulmonary ligament was covered by a monolayer of mesothelial cells (Fig. 4). In the immunohistochemical studies, the positive and negative controls yielded the appropriate reactions. The mesothelial cells were immunohistochemically positive for CAM5.2 (Fig. 4D) and D2-40 (Fig. 4E) and negative for CD31. Beneath the mesothelial layer, we observed an abundance of cistern-related dilated lymphatic capillaries. The endothelial cells of these lymphatic capillaries were immunohistochemically positive for D2-40 (Fig. 4E) and CD31 (Fig. 4F) and negative for CAM5.2 (Fig. 4D). Between the mesothelial layer and the submesothelial lymphatic capillaries, we observed a thin fibrous connective tissue that was discontinuous and formed apertures that communicated directly with the pleural cavity. These apertures

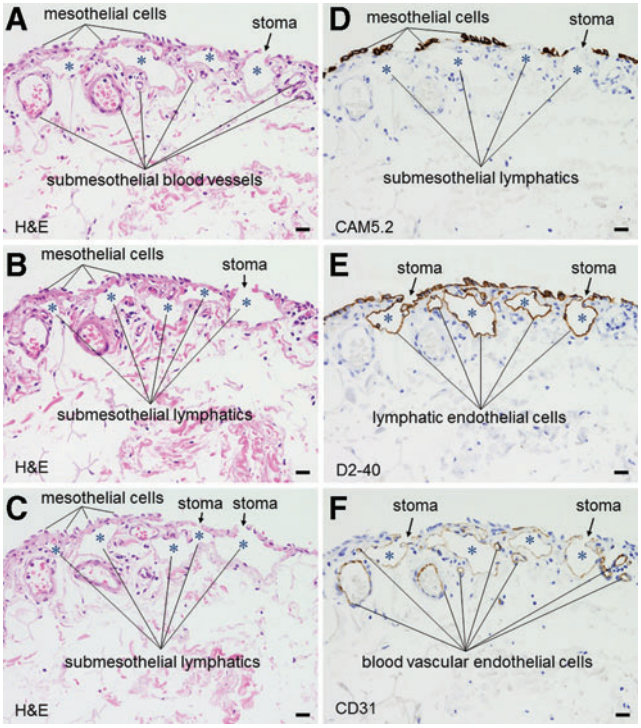

FIG. 4. Light micrographs of serial sections of the pulmonary ligament. The submesothelial layer consists of fibrous connective tissue, which is occasionally discontinuous due to interruptions by stomata. The stomata are lined with low-molecular weight cytokeratin CAM5.2(-), D2-40(+), and CD31(+) lymphatic endothelial cells (**A, B, and C;** hematoxylin and eosin staining, objective 20X) (**D, E and F**, immunohistochemistry, low-molecular weight cytokeratin CAM5.2, D2-40, and CD31, respectively, objective 20X). *Asterisks* indicate submesothelial lymphatic lumens. The scale bars indicate 20 μm. A color version of this figure is available in the online article at www.liebertpub.com/lrb

were fringed with D2-40-positive, CD31-positive, and CAM5.2-negative lymphatic endothelial cells (Fig. 4). An immunofluorescent multiple staining method highlighted these structures (Fig. 5). Three-dimensional histological image reconstruction of the pulmonary ligament indicated the proximity of the lymphatics to the mesothelial layer and submesothelial-rich lymphatics that were irregularly dilated, cistern-related or anastomotic (Fig. 6).

The sizes and densities of these apertures varied from case to case (Table 2). The median aperture sizes ranged from 2.25 to 8.75 μm in the left pulmonary ligaments and from 2.50 to 12.50 μm in the right pulmonary ligaments. The aperture densities ranged from 2 to 9 per mm^2 in the left pulmonary ligaments and from 2 to 18 per mm^2 in the right pulmonary ligaments. However, no significant differences were found in the sizes ($n=11$, $p=0.359$) or densities ($n=11$, $p=0.438$) of the apertures between the left and right pulmonary ligaments.

Discussion

In the present study, the apertures exhibited structural adequacy as lymphatic stomata on the surface of the pulmonary ligament in adult humans, thereby providing evidence of lymphatic stomata in the adult human pleura.

In the serosal membrane, the term *stomata* has historically been used to describe the following three microstructures: 1) gaps formed in the submesothelial connective tissue that do not directly communicate with submesothelial lymphatics but may constitute a pre-lymphatic fluid pathway, which is often referred to as *macula cribriformis*;[28,29] 2) apertures in which the lymphatic endothelial cells are exposed to the serosal cavity without patency but are accompanied with a flap valve-related intercellular overlapping of endothelial cells, which is occasionally referred to as closed lymphatic stomata;[30,31] and 3) apertures fringed with lymphatic endothelial cells that enable direct communication between the lymphatic lumen and the serosal cavity,[32] which is occasionally referred to as open

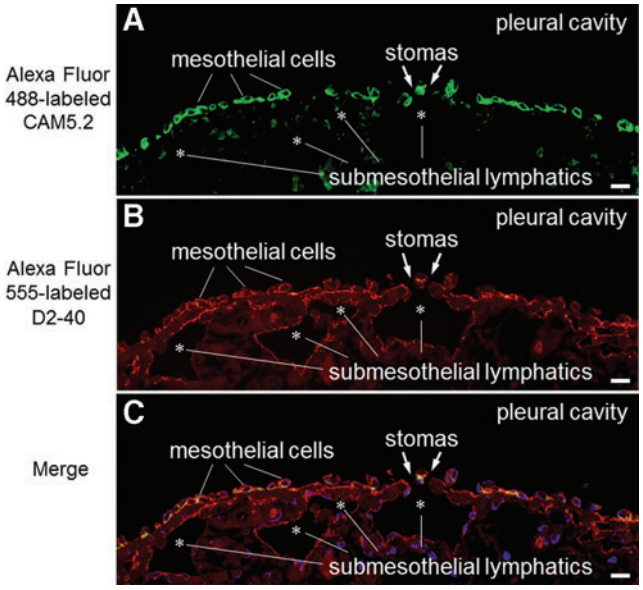

FIG. 5. Low-power photomicrographs of immunofluorescent multiple staining performed on the pulmonary ligament (fluorescence microscope). This tissue section is one of the serial sections following Figure 4C. **(A)** The *green-colored cells* indicate mesothelial cells that react with low-molecular weight cytokeratin CAM5.2 antibody. **(B)** The *orange-colored cells* indicate mesothelial cells and lymphatic endothelial cells that react with D2-40 antibody. **(C)** The *yellow-* or *green-colored cells* represent mesothelial cells, and the *orange-colored cells* represent lymphatic endothelial cells. *Asterisks* indicate submesothelial lymphatic lumens. The scale bars indicate 20 μm. A color version of this figure is available in the online article at www.liebertpub.com/lrb

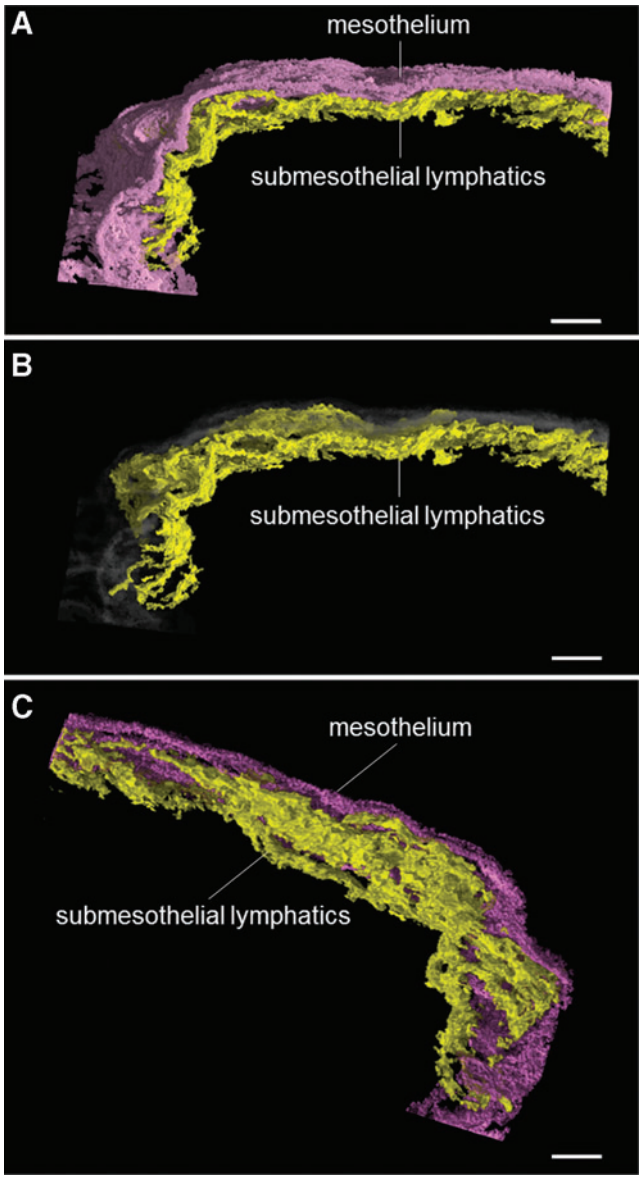

FIG. 6. Three-dimensional histological image reconstruction of the mesothelium and lymphatics in the pulmonary ligament. The *violet color* denotes mesothelial cells, the *yellow color* denotes lymphatic endothelial cells, and the *gray color* indicates the transparent image of mesothelial cells. **(A)** and **(B)** The proximity of the lymphatics to the mesothelial layer can be observed (*horizontal view*). **(C)** The submesothelial lymphatic vessels reveal irregularly dilated and anastomotic structures, forming a rich lymphatic network (*diagonal view* from the submesothelial side). The scale bars indicate 100 μm. A color version of this figure is available in the online article at www.liebertpub.com/lrb

Table 2. Size of Apertures on the Pulmonary Ligaments

	Size of apertures on the left pulmonary ligament (μm)							*Size of apertures on the right pulmonary ligament (μm)*						
Case	*Median*	*Mean*	*Minimum*	*Maximum*	*SE*	*SD*	*(n)*	*Median*	*Mean*	*Minimum*	*Maximum*	*SE*	*SD*	*(n)*
1	4.00	5.04	2.25	10.00	1.28	3.13	6	5.00	7.00	5.00	10.00	1.22	2.74	5
2	5.00	4.17	2.50	5.00	0.83	1.44	3	12.50	12.08	2.50	20.00	3.25	7.97	6
3	3.25	3.25	2.50	4.00	0.75	1.06	2	5.00	5.00	2.50	7.50	2.50	3.54	2
4	7.50	9.21	2.00	20.00	2.40	6.34	7	5.00	9.78	2.00	35.00	2.47	10.48	18
5	2.50	3.00	2.00	5.00	0.68	1.35	4	2.38	2.79	2.00	5.00	0.47	1.14	6
6	2.25	2.20	2.00	2.50	0.09	0.21	5	2.50	4.54	2.00	12.50	1.52	4.02	7
7	2.50	2.97	2.00	5.00	0.40	1.19	9	5.00	4.92	2.25	7.50	1.52	2.63	3
8	5.00	5.83	2.50	10.00	2.20	3.82	3	3.75	4.38	2.50	7.50	1.20	2.39	4
9	3.00	7.10	2.50	15.00	2.74	6.14	5	2.50	3.33	2.50	5.00	0.83	1.44	3
10	3.75	3.63	2.00	5.00	0.80	1.60	4	4.50	4.38	2.50	6.00	0.75	1.49	4
11	2.50	3.33	2.50	5.00	0.83	1.44	3	2.50	5.00	2.50	10.00	2.50	4.33	3
12	n/e	n/e	n/e	n/e	n/e	n/e	n/e	7.25	10.65	5.00	27.50	2.29	7.23	10
13	5.00	6.50	2.50	12.50	1.70	3.79	5	n/e	n/e	n/e	n/e	n/e	n/e	n/e
14	n/e	n/e	n/e	n/e	n/e	n/e	n/e	3.75	5.63	2.50	12.50	2.37	4.73	4
15	8.75	9.17	2.50	15.00	1.79	4.38	6	n/e	n/e	n/e	n/e	n/e	n/e	n/e

n/e = not evaluated because of pleural adhesion. (n) = frequency of apertures observed per 1 mm^2.

lymphatic stomata. The structural and immunohistochemical properties of the apertures observed in the present study were consistent with those of open lymphatic stomata.

In various types of mammalian pleural cavities, lymphatic stomata are exclusively observed in the parietal pleura and are considered to be a major route for pleural fluid resorption and the egress of cells or foreign particles.[33,34] Pleural effusion occurs when the entry rate of liquid increases, the exit rate of liquid decreases, or a combination of both.[5] Given that lymphatics in the parietal pleura have a large capacity with respect to the exit rate (0.28 mL/kg/h, which is nearly 30 times the baseline rate of 0.01 mL/kg/h), a situation in which only the entry rate increased would require a sustained rate of greater than 30 times the normal rate to exceed the reserve lymphatic drainage capacity. However, if the exit rate exclusively decreased, it would require more than a month at the normal entry rate of 12 ml/day to produce an effusion detectable by chest radiograph.[5] It is also important to note that a portion of foreign particles inhaled and deposited into the lung is thought to reach the pleura, pass through the pleural space, and exit via the stomata.[35] Interestingly, long fibers and long carbon nanotubes, such as asbestos fibers, cannot negotiate the stomata and are retained, thus initiating inflammation and pleural pathology.[36] Therefore, lymphatic stomata are considered to be directly or indirectly involved in certain pleural diseases.

The physiological mechanism of intrapleural drainage via lymphatic stomata has not been established. In general, lymphatics are thought to have two types of valve systems: a flap valve system and an outlet valve system.[37,38] The former consists of overlapping of adjacent lymphatic endothelial cells with a loose, button-like junction at the initial lymphatics that allows fluid to enter from the interstitium into the lymphatics but prevents reflux.[37] The latter consists of plicae of the lymphatic inner wall that are typically preset as a set of two semilunar, pocket-like structures facing each other in the lymphatic lumen.[38] This outlet valve prevents reflux between adjacent lymphangions and enables unidirectional lymph flow in collaboration with a pumping action of the lymphatic vessels.[38]

Of particular note is that the lymphatic vessels effectively adapt their contractile force to the particular hydrodynamic conditions according to different anatomical regions.[39] With regard to the pleural cavity, the intrapleural pressure and surface area of the pleura vary dynamically depending on a number of factors, such as breathing patterns and physical exertion. For example, the mean cephalocaudal distances during motion of the central portion of the diaphragm where the lower portion of the pulmonary ligament is attached are approximately 20.6 mm during spontaneous breathing and 64.2 mm during maximal deep breathing in healthy younger adults.[40] Several investigators have speculated that back-flow from the lymphatic stomata into the serosal cavity is prevented by minute overlapping of mesothelial and endothelial cells according to serosal membrane movement that is synchronously coordinated during breathing;[41–43] whether this cellular overlapping in the lymphatic stomata can efficiently prevent regurgitation against these dynamic changes remains to be determined. Because not all of the stomata we observed were equipped with flap valve-related cytoplasmic processes, some of the flow via the stomata is potentially bidirectional.

Although the role of the pulmonary ligament remains to be completely elucidated, it does play a significant role in influencing the presentation and configuration of many events that affect the lower lobe, the adjacent pleural space, and the mediastinum.[23] Some of the lymph from the lower lobe of the lung flows into the pulmonary ligament;[44] a lymph node chain is present in the pulmonary ligaments of the lung where the lymph nodes correspond to station 9.[45] The lymphatic vessels of the pulmonary ligament drain toward the tracheal bifurcation, the thoracic duct, or the intra-abdominal lymph nodes in the celiac region.[45] Interestingly, these lymph flows can travel bi-directionally even under normal conditions.[46–51] In addition, cancer metastasis to the pulmonary ligament has a potential role in the pathogenesis of pleural carcinomatosis.[22] The functional roles of the pulmonary ligament must be explored from the perspective of the lymphatic stomata.

In conclusion, our study has confirmed the presence of lymphatic stomata in the adult human pleura. Understanding

the properties of these structures under normal and abnormal conditions will help to elucidate several mechanisms of human pleural diseases.

Acknowledgments

We thank the following individuals at Tokyo Medical University for sharing their expertise on human anatomical pathology: Motoshige Kudo, MD, PhD; Reisuke Takahashi, MD, PhD; Isao Yoshihama, PhD; and the late Yoshiro Ebihara, MD, PhD. We also thank Michiyo Kanazawa, LT; Yukiko Nishio, LT; Hiroyuki Machida, MD, PhD; Hajime Kitamura, MD, PhD; Shoji Yamanaka, MD, PhD; Yoshiaki Inayama, MD, PhD; and the late Kiyoshi Gomi, MD, PhD at Yokohama City University for providing technical advice. Finally, we thank Edward F. Barroga, DVM, PhD, and J. Patrick Barron, Professor Emeritus at Tokyo Medical University for reviewing our manuscript, as well as Tatsuo Shimada, MD, PhD, at Matrix Medicine, Faculty of Medicine, Oita University for providing constructive criticism.

Author Disclosure Statement

No competing financial interest exists. This research was supported by Grants-in-Aid for Scientific Research from the Ministry of Education, Culture, Sports, Science and Technology of Japan (No. 20790993 and No. 24590242 to H.O.), Exploratory Research from the Yokohama Foundation for Advancement of Medical Science (to H.O.), and Medical Research from the Tokyo Medical University Cancer Center (to H.O.).

References

1. Mactier RA, Khanna R. Peritoneal lymphatics. In: Gokal R, Nolph KD, eds. *The Textbook of Peritoneal Dialysis.* Norwell: Kluwer Academic Publishers; 1994: pp. 115–134.
2. Lay-Fook SJ. Pleural mechanics and fluid exchange. Physiol Rev 2004;84:385–410.
3. Raybuck HE, Allen L, Harms WS. Absorption of serum from the peritoneal cavity. Am J Physiol 1960;199:1021–1024.
4. Nagy JA. Lymphatic and nonlymphatic pathways of peritoneal absorption in mice: physiology versus pathology. Blood Purif 1992;10:148–162.
5. Broaddus VC, Light RW. Pleural effusion. In: Mason RJ, Broaddus VC, Martin TR, King Jr. TE, Schraufnagel DE, Murray JF, Nadel JA, eds. *Murray and Nadel's Textbook of Respiratory Medicine,* 5th edition, Volume II. Philadelphia: Saunders Elsevier; 2010: pp. 1719–1763.
6. Wang PM, Lai-Fook SJ. Regional pleural filtration and absorption measured by fluorescent tracers in rabbits. Lung 1999;177:289–309.
7. Ohtani O, Ohtani Y. Organization and developmental aspects of lymphatic vessels. Arch Histol Cytol 2008;71:1–22.
8. Von Recklinghausen FD. Zur Fettresorption. Virchows Arch 1863;26:172–208.
9. Wang NS. The preformed stomas connecting the pleural cavity and the lymphatics in the parietal pleura. Am Rev Respir Dis 1975;111:12–20.
10. Pinchon MC. Pleural permeability in the rat. I. Ultrastructural basis. Biol Cell 1980;37:269–272.
11. Wang QX, Ohtani O, Saitoh M, Ohtani Y. Distribution and ultrastructure of the stomata connecting the pleural cavity with lymphatics in the rat costal pleura. Acta Anat (Basel) 1997;158:255–265.
12. Mariassy AT, Wheeldon EB. The pleura: A combined light microscopic, scanning, and transmission electron microscopic study in the sheep. I. Normal pleura. Exp Lung Res 1983;4:293–314.
13. Albertine KH, Wiener-Kronish JP, Staub NC. The structure of parietal pleura and its relationship to pleural liquid dynamic in sheep. Anat Rec 1984;208:401–409.
14. Masada S, Ichikawa S, Nakamura Y, Uchino S, Kato H. Structure and distribution of the lymphatic vessels in the parietal pleura of the monkey as studied by enzyme-histochemistry and by light and electron microscopy. Arch Histol Cytol 1992;55:525–538.
15. Miura T, Shimada T, Tanaka K, Chujo M, Uchida Y. Lymphatic drainage of carbon particles injected into the pleural cavity of the monkey, as studied by video-assisted thoracoscopy and electron microscopy. J Thorac Cardiovasc Surg 2000;120:437–447.
16. Shinohara H. Distribution of lymphatic stomata on the pleural surface of the thoracic cavity and the surface topography of the pleural mesothelium in the golden hamster. Anat Rec 1997;249:16–23.
17. Rahman NM, Wang NS. Anatomy of the pleura. In: *Textbook of Pleural Diseases.* Light RW, Lee G, eds. Boca Raton: CRC Press; 2008: pp. 13–25.
18. Broaddus VC, Wiener-Kronish JP, Berthiaume Y, Staub NC. Removal of pleural liquid and protein by lymphatics in awake sheep. J Appl Physiol 1988;64:384–390.
19. Zarogiannis S, Hatzoglou C, Gourgoulianis K, Molyvdas PA. Role of human visceral pleura in pleural fluid turnover: Need for morphological evidence of lymphatic stomata. Chin Med J 2006;119:1495–1496.
20. Gaudio E. Rendina EA, Pannarale L, Ricci C, Marinozzi G. Surface morphology of the human pleura: a scanning electron microscopic study. Chest 1988;93:149–153.
21. Peng MJ, Wang NS, Vargans FS, Light RW. Subclinical surface alterations of human pleura: A scanning electron microscopic study. Chest 1994;106:351–353.
22. Liu S, Oshiro H, Kato Y, Kudo M, Ebihara Y. The role of the pulmonary ligament in the pathogenesis of pleural carcinomatosis. Jpn J Lung Cancer 2001;41:643–648.
23. Rabinowitz JG, Cohen BA, Mendleson DS. Symposium on nonpulmonary aspects in chest radiology. The pulmonary ligament. Radiol Clin North Am 1984;22:659–672.
24. Ji RC, Miura M, Qu P, Kato S. Expression of VEGFR-3 and 5′-nase in regenerating lymphatic vessels of the cutaneous wound healing. Microsc Res Tech 2004;64:279–286.
25. Oshiro H, Odagaki Y, Iobe H, Ozu C, Takizawa I, Nagai T, Matsubayashi J, Inagaki A, Miyake S, Nagao T. Primary large cell neuroendocrine carcinoma of the ureter. Int J Clin Exp Pathol 2013;6:729–736.
26. Machida H, Ito S, Hirose T, Takeshita F, Oshiro H, Nakamura T, Mori M, Inayama Y, Yan K, Kobayashi N, Yokota S. Expression of Toll-like receptor 9 in renal podocytes in childhood-onset active and inactive lupus nephritis. Nephrol Dial Transplant 2010;25:2530–2537.
27. Aoba T, editor. *Three-Dimensional Motion View of Tissue Architectures and Lesions.* Tokyo: Ishiyaku Publishers; 2009.
28. Kihara T. extravaskuläre Saftbahnsystem [The extravascular fluid pathway system]. Okajima Folia Anat Jpn 1956;28:601–621.
29. Shimada T, Zhang L, Oya M. Architecture and function of the extravascular fluid pathway: Special reference to the

macula cribriformis in the diaphragm. Kaibogaku Zasshi 1995;70:140–155.
30. Shinohara H, Fukuo Y, Matsuda T. On the presence and function of closed lymphatic stomata in the diaphragm of the golden hamster. Okajimas Folia Anat Jpn 1989;66:69–79.
31. Huang C-T, Iimura A. Stomata and lymphatic vessels in rat costal pleura. Jpn J Lymphol 1992;15:1–11.
32. Ohtani Y, Ohtani O, Nakatani T. Microanatomy of the rat diaphragm: A scanning electron and confocal laser scanning microscopic study. Arch Histol Cytol 1993;56:317–328.
33. Brotons ML, Bolca C, Fréchette E, Deslauriers J. Anatomy and physiology of the thoracic lymphatic system. Thorac Surg Clin 2012;22:139–153.
34. Yalcin NG, Choong CK, Eizenberg N. Anatomy and pathophysiology of the pleura and pleural space. Thorac Surg Clin 2013;23:1–10.
35. Donaldson K, Murphy FA, Duffin R, Poland CA. Asbestos, carbon nanotubes and the pleural mesothelium: A review of the hypothesis regarding the role of long fibre retention in the parietal pleura, inflammation and mesothelioma. Part Fibre Toxicol 2010;7:5.
36. Murphy FA, Poland CA, Duffin R, Al-Jamal KT, Ali-Boucetta H, Nunes A, Byrne F, Prina-Mello A, Volkov Y, Li S, Mather SJ, Bianco A, Prato M, Macnee W, Wallace WA, Kostarelos K, Donaldson K. Length-dependent retention of carbon nanotubes in the pleural space of mice initiates sustained inflammation and progressive fibrosis on the parietal pleura. Am J Pathol 2011;178:2587–2600.
37. Schmid-Schönbein GW. The second valve system in lymphatics. Lymphat Res Biol 2003;1:25–29; discussion 29–31.
38. Zawieja DC. Contractile physiology of lymphatics. Lymphat Res Biol 2009;7:87–96.
39. Gashev AA, Zhang RZ, Muthuchamy M, Zawieja DC, Davis MJ. Regional heterogeneity of length-tension relationships in rat lymph vessels. Lymphat Res Biol 2012;10:14–19.
40. Tomita K, Sakai Y, Monma M, Ohse H, Imura S. Dynamic MRI of normal diaphragmatic motions during spontaneous breathing and maximal deep breathing. Rigakuryoho Kagaku 2004;19 237–243.
41. Bettendorf U. Electron microscopic studies on the peritoneal resorption of intraperitoneally injected latex particles via the diaphragmatic lymphatics. Lymphology 1979;12:66–70.
42. Tsilibary EC, Wissig SL. Lymphatic absorption from the peritoneal cavity: Regulation of patency of mesothelial stomata. Microvasc Res 1983;25:22–39.
43. Tsilibary EC, Wissig SL. Light and electron microscope observations of the lymphatic drainage units of the peritoneal cavity of rodents. Am J Anat 1987;180:195–207.
44. Okada Y, Ito M, Nagaishi Ch. Anatomical study of the pulmonary lymphatics. Lymphology 1979;12:118–124.
45. Riquet M. Lung cancer and lymph drainage. Cancer Radiother 2007;11:4–10.
46. Baltaxe HA, Constable WC. Mediastinal lymph node visualization in the absence of intrathoracic disease. Radiology 1968;90:94–98.
47. Weidner WA, Steiner RM. Roentgenographic demonstration of intrapulmonary and pleural lymphatics during lymphangiography. Radiology 1971;100:533–539.
48. Grant T, Levin B. Lymphangiographic visualization of pleural and pulmonary lymphatics in a patient without chylothorax. Radiology 1974;113:49–50.
49. Cha EM, Sirijintakarn P. Anatomic variation of the thoracic duct and visualization of mediastinal lymph nodes: A lymphographic study. Radiology 1976;119:45–48.
50. Clark RA, Colley DP. Pulmonary lymphatics visualized during pedal lymphangiography. Radiology 1980;136:29–32.
51. Rino Y, Imada T, Takanashi Y, Kobayashi O, Sairenji M, Motohashi H. Route from the paraaortic lymphatic system to the tracheobronchial lymph nodes evidenced on lymphangiogram in a patient with gastric cancer. Gastric Cancer 2004;7:176–177.

Address correspondence to:
Hisashi Oshiro, MD, PhD
Department of Anatomic Pathology
Tokyo Medical University
6-7-1 Nishi-shinjuku
Shinjuku, Tokyo 1600-023
Japan

E-mail: oshiroh@yokohama-cu.ac.jp